

Mesoscopic simulations of phase distribution effects on the effective thermal conductivity of micro granular porous media

Moran Wang^{1†}, Ning Pan¹, Jinku Wang², Shiyi Chen³

¹*Department of Biological & Agricultural Engineering, University of California, Davis, CA 95616, USA*

²*School of Aerospace, Tsinghua University, Beijing 100084, China*

³*Department of Mechanical Engineering, the Johns Hopkins University, Baltimore, MD 21218, USA*

Cited as:

Moran Wang, Ning Pan, Jinku Wang, Shiyi Chen. Mesoscopic simulations of phase distribution effects on the effective thermal conductivity of microgranular porous media. *Journal of Colloid and Interface Science*, Volume 311, Issue 2, 15 July 2007, Pages 562-570

[†] Email address: mmwang@ucdavis.edu

Abstract

This paper analyzes the phase distribution effects on the effective thermal conductivity (ETC) of multiphase micro granular porous media using mesoscopic statistics based numerical methods. A multi-parameter random generation-growth method, Quartet Structure Generation Set (QSGS), is developed for replicating microstructures of multiphase granular porous media based on the macroscopic statistical information, such as the volume fractions and the phase interactions. The phase distribution characteristics and the interphase connections are controlled by adjusting the related parameters. Then the energy transport equations through porous media are solved by a lattice Boltzmann method developed by us with multiphase conjugate heat transfer considered. The results indicate that a smaller average particle size could lead to a larger effective thermal conductivity of two-phase porous media for a certain porosity. For the anisotropic media, if the larger directional growth probability is along the direction of temperature gradient, the effective thermal conductivity in the parallel direction is enhanced as a result, and that in the vertical direction will be weakened. For multiphase porous media, the degree of phase conglomeration is determined by the phase interactions. A larger liquid-liquid interaction leads to a higher degree of liquid phase conglomeration and therefore a larger effective thermal conductivity of the porous media.

Keywords: effective thermal conductivity; micro porous media; phase distribution; anisotropy

1. Introduction

The thermal properties of porous media have been of great interests recently due to their applications in science and engineering, such as material design, geophysical exploration, biological and medical engineering [1-8]. Most previous theoretical models for predicting the effective thermal conductivities (ETC) are based on the network combinations of Series and Parallel models [9-12] or on the uniform phase assumption [12]. Although these models are easy to use because of their simple dependence on phase fractions, the effects of phase distribution and multiphase interaction on the effective thermal conductivities are yet ignored. A full numerical determination of thermal properties of porous media generally includes two steps: Acquiring the structure and phase distribution information into consideration and then solving the relevant set of local energy transport equations.

Several methods have been proposed to generate microstructures of multiphase materials in the past decade. Tacher *et al.* [13] presented a discrete reduced distance method to generate spherical/elliptical two-phase granular porous media. Based on Tacher's work, Pilotti developed a grains sedimentation algorithm [14]. Both Tacher's and Pilotti's methods generate porous media with random size and locations, however, neither can deal well with the connections between grains. Therefore neither is suitable for the heat transfer problems which are extremely sensitive to connections. Recently, the reconstruction process has been widely used in generating random two-phase [15,16] and multi-component [17,18] porous materials based on the digital micro-tomographic information and statistical correlation functions [19]. This kind of reconstruction method is more suitable for non-fluidic or single-fluid systems but not for multiple fluid systems. Mohanty [20] therefore generated unsaturated porous media using a Monte Carlo annealing algorithm based on the law of lowest interfacial energy. However, one can notice from the available data and images that the lowest-energy law is, but not always, the rule dominating the phase distributions of porous media where random factors may play more important roles, especially in micro porous media [18]. Wang *et al.* [21,22] proposed a multi-parameter random generation-growth method, termed Quartet Structure Generation Set (QSGS), to replicate randomly

distributed multiphase granular porous media based on the cluster growth theory [22,7] and then investigated the thermal conductivity of isotropic porous media.

To solve the relevant set of local energy transport equations, the traditional partial differential equation (PDE) solvers, such as finite difference method (FDM) and finite element method (FEM), have been applied for the first steps [24-26]. However, such traditional PDE solvers demand huge or often unacceptable computational resources when the porous structure becomes complicated, especially when the fluid-solid conjugate heat transfer problem is considered [27,28]. Meanwhile the stochastic methods for representing the perturbations in porous media have gained much attention recently [29,30]. Shoshany et al. [31] and Barta & Dieska [32] modeled the thermal conductivity of porous materials using the Monte Carlo methods to reflect the structural fluctuations during the process. Zhang *et al.* [33,34] developed a randomly mixed material model (RMM) for predicting the effective thermal conductivity of moist porous media. Qian *et al.* [35] proposed a two dimensional five-speed (D2Q5) lattice Boltzmann model to simulate the effective thermal conductivity of porous media, while neglecting the solid-fluid conjugate heat transfer, which actually plays a critical role in thermal transport in porous media [36,37].

Following our previous work, we develop the QSGS further for generating microstructures of multiphase porous media with emphasis on the parameter effects on phase distributions. After the microstructures of porous media are generated, the thermal conduction equations are solved by a lattice Boltzmann method with multiphase conjugate heat transfer effects considered. The phase distribution effects on the ETC of micro granular porous media are thus analyzed.

2. Numerical Methods

2.1 Randomly generation-growth algorithm for generating porous structures

Before the generation, one needs to determine which phase is the non-growing phase and then the rests are growing phases. In the present paper, we call the non-growing phase the first phase, and the growing phase as the n -th phase, where $n = 2$ to N , the total number of phases in the system. Without

losing generality, the discrete phases are normally taken as the growing phases. For example, rocks and water are the growing phases in unsaturated sands, while the gas is the growing phase for the polyurethane foams.

The QSGS for generating porous structures includes six steps [21]:

i) Randomly locate the cores of the first growing phase in a grid system based on a core distribution probability, c_d , whose value is no greater than the volume fraction of the phase. Each cell in the grid will be assigned a random number by a uniform distribution function within (0, 1). Each cell whose random number is no greater than c_d will be chosen as a core;

ii) Enlarge every element of the growing phase to its neighboring cells in all directions based on each given directional growth probability, D_i , where i represents the direction. Again for each growing element, new random numbers will be assigned to its neighboring cells. The neighboring cell in direction i will become part of the growing phase if its random number is no greater than D_i ;

iii) Repeat the growing process of *ii)* until the volume fraction of the first growing phase reaches its given value P^2 (if the growing phase is gas, P^2 is more often expressed as the porosity ε);

iv) As to the next growing phase, there are two cases to consider depending on its interaction with the existing phase(s). If this phase is an equivalent discrete phase as the existing growing phase, such as multi-component mixture, it grows from separate seeds, which is very similar as the first growing phase described in *i)-iii)*. Otherwise, we have to consider the constraint by and interaction with the existing phase(s). For such cases, the n -th phase ($n > 2$) will grow based on a phase interaction growth probability, $I_i^{n,m}$, which represents the growth probability of the n -th phase on the m -th phase along the i -th direction;

v) Stop the n -th phase growth once its volume fraction reaches the given value P^n .

vi) Repeat the next phase growth as described in *iv)* & *v)* until $n = N$. The spaces not occupied at the end represent the non-growing phase.

Thus, there are four parameters ($c_d, D_i, P^n, I_i^{n,m}$) controlling the microstructures of generated porous media based on the generation process. The core distribution probability c_d is defined as the probability of a cell to become a core of the first growing phase on which growth or expansion of the first phase originates. The value of c_d indicates the number density of growing cores for the first growing phase, to reflect the statistical distribution of the first growing phase throughout the system. The c_d value thus also controls the degree of structure details of a system; a smaller c_d leads to a finer description of the microstructures including particle/pore shapes and inter-particle/pore connections, etc. However a small c_d value will also decrease the statistical particle numbers for a given grid size and thus increase the computation fluctuation.

The directional growth probability D_i is defined as the probability for a yet to be occupied cell to merge into a neighboring cell in the i -th direction to become part of the growing phase. An appropriate arrangement of the directional growth probabilities may lead to an isotropic structure. In other words, the growth probabilities can be adjusted to control the degree of anisotropy. For two-dimensional cases, each square cell has eight growing directions to its neighbors, as seen in Fig. 1. There are four main directions (1,2,3,4) and four diagonal directions (5,6,7,8). To obtain an isotropic structure in such systems, we set both the main directional growth probabilities D_{1-4} and the diagonal directional growth probabilities D_{5-8} into respective constant in each group, and the both constants in a fixed ratio. For instance by designating the probabilities ratio, $D_{1-4} : D_{5-8} = 4$, we get the directional growth probability consistent with the equilibrium density distribution function for isotropic materials [38,39].

For multiphase porous media systems ($n > 2$), the interactions between different discrete phases become even more complex, and we have to consider the effects of such interactions during the phase growth. Such effects are important especially for instance in unsaturated porous media soaked by a liquid that wets other phases in the system differently. In such systems, the growth order of the various phases is

important. Generally the solid phase is selected as the first growing phase and then the liquid phase grows under the influences of phase interactions. The phase interaction growth probability, $I_i^{n,m}$ i.e., the growth probability of n -th phase on the surface of m -th phase along the i -th direction, is hence introduced to account for this influence by assigning different values to $I_i^{n,m}$ for different materials. The value of the phase interaction growth probability $I_i^{n,m}$ could be determined by analyzing the scanned pictures of phase distributions or by calculating from the wetting properties directly.

Comparing with the existing generation methods, the QSGS may have following merits: i) The generation-growth process is very close to the natural formation process of most real porous media which grow outward from cores. Therefore the generated microstructure is more realistic. ii) Each of the parameters in the algorithm has a distinct physical significance, instead of an empirical determination. iii) It deals well with multi-body connection problems. iv) The stochastic and statistical features of system are determined before the treatment by the physical laws, instead of other way around as in many existing methods, thus facilitating smoother tackling of the physical problems in a more realistic setting (the material is already there before modeling). v) The method is efficient without turning to any iteration process. The algorithm is straightforward in three-dimensional and/or multiphase cases, and suitable for parallel computing.

2.2 Lattice Boltzmann algorithm for solving energy equations

The lattice Boltzmann method (LBM) is intrinsically a mesoscopic approach based on the evolution of statistical distribution on lattices, and has achieved considerable success in simulating fluid flows and associated transport phenomena [40-43]. The most important advantages of the LBM are the easy implementations of multiple inter-particle interactions and complex geometry boundary conditions [44-46], and the conservation laws can hold automatically in general without additional computational efforts [47]. The LBM thermal models have been developed recently [48,49]. Here we introduce our previous

lattice Boltzmann algorithm for fluid-solid conjugate heat transfer [37], and adapt it for effective thermal conductivity predictions.

For a pure thermal conduction in porous media with no phase change, no heat source and no convection, the temperature evolution equation for each phase is generally written as,

$$g_{\alpha}(\mathbf{r} + \mathbf{e}_{\alpha} \delta_t, t + \delta_t) - g_{\alpha}(\mathbf{r}, t) = -\frac{1}{\tau_n} [g_{\alpha}(\mathbf{r}, t) - g_{\alpha}^{eq}(\mathbf{r}, t)], \quad (1)$$

which is actually a simplified form for multiphase conjugate heat transfer by eliminating the convection and heat source terms [37]. The equilibrium distribution of the evolution variable, g_{α} , for the two dimensional nine-speed (D2Q9) model is

$$g_{\alpha}^{eq} = \begin{cases} 0 & \alpha = 0 \\ T/6 & \alpha = 1, 2, 3, 4 \\ T/12 & \alpha = 5, 6, 7, 8 \end{cases}, \quad (2)$$

the microscopic velocity

$$\mathbf{e}_{\alpha} = \begin{cases} (0, 0) & \alpha = 0 \\ (\cos \theta_{\alpha}, \sin \theta_{\alpha})c & \theta_{\alpha} = (\alpha - 1)\pi/2 & \alpha = 1, 2, 3, 4, \\ \sqrt{2}(\cos \theta_{\alpha}, \sin \theta_{\alpha})c & \theta_{\alpha} = (\alpha - 5)\pi/2 + \pi/4 & \alpha = 5, 6, 7, 8 \end{cases} \quad (3)$$

and the dimensionless relaxation time

$$\tau_n = \frac{3}{2} \frac{k_n}{(\rho c_p)_n c^2 \delta_t} + 0.5, \quad (4)$$

where the subscript n still represents the n -th phase, δ_t the time step, k the thermal conductivity, and c a *pseudo* sound speed whose value can take any positive value theoretically only to insure τ values within (0.5, 2) [42]. To meet the requirement of temperature and heat flux continuities at phase interfaces, we have to assume identical volume thermal capacities (ρc_p) for different phases; the conjugate heat problem between different phases is thus solved and these assumptions will not affect the effective thermal conductivity calculated [36]. The temperature and the heat flux are then calculated by

$$T = \sum_{\alpha} g_{\alpha} \quad (5)$$

$$q = \left(\sum_{\alpha} \mathbf{e}_{\alpha} g_{\alpha} \right) \frac{\tau_n - 0.5}{\tau_n} \quad (6)$$

For the isothermal boundary treatment, we follow the bounce-back rule of the non-equilibrium distribution proposed by Zou and He [50]:

$$g_{\alpha} - g_{\alpha}^{eq} = - \left(g_{\beta} - g_{\beta}^{eq} \right) \quad (7)$$

where the subscripts α and β represent two opposite directions respectively, and the equilibrium distribution can be calculated using the local boundary temperatures.

For the insulated boundary, we have tried the Neumann boundary treatment [37] and let the boundary temperature gradient equal to zero. However heat flux leak will result along the insulated surfaces. Therefore a specular reflection boundary condition is implemented here

$$g_{\alpha} = g_{\beta} \quad (8)$$

After the temperature field is solved, the ETC, k_{eff} , can finally be determined as:

$$k_{eff} = \frac{L \cdot \int q \cdot dA}{\Delta T \int dA} \quad (9)$$

where q is the steady heat flux through the media cross section area dA between the temperature difference ΔT with a distance L .

3. Validations

To validate the present methods for calculating the effective thermal conductivity of micro porous media, this section compares the numerical results with the existing theoretical solutions and experimental data.

3.1 Theoretical solutions

[Insert Figure 2 here]

First we validate the numerical solver by calculating the effective thermal conductivities for two basic structures of double-component materials: the Parallel mode and the Series mode (see Fig. 2). Assuming the thermal conductivity of each component is k_1 and k_2 respectively, the simple theoretical solutions give the effective thermal conductivities as $(k_1 + k_2)/2$ for the Parallel mode and $1/(1/2k_1 + 1/2k_2)$ for the Series mode.

[Insert Table 1 here]

Table 1 lists the calculated effective thermal conductivities comparing with theoretical solutions for different values of k_2 . k_1 is kept constant as 1.0 W/m·K while k_2 changes from 2.0 to 1000 W/m·K. The results show the deviations are no greater than 0.02% for the Parallel mode and 0.25% for the Series mode, which indicates good accuracy of the present numerical solver.

3.2 Experimental data

Second we combine the QSGS for generating random multiphase structure with the LBM solver for solving the energy transport equations together, and then predict the effective thermal conductivity of heterogeneous materials. The numerical results are compared with two experimental cases.

Consider a two-phase composite, Cu/solder where the Cu particles are uniformly dispersed in the solder mass. The solder is selected as the non-growing (first) phase and the Cu particles are the growing (second) phase. The component thermal conductivities are $k_{Cu}=398.0$ W/m·K and $k_{solder}=78.1$ W/m·K. Fig. 3 shows the predicted effective thermal conductivities as a function of Cu volume fraction, $P_2(\varepsilon)$, which are compared with the experimental data from [51]. The phase distribution details are unknown so that we have to make common-sense estimates. The parameters used in present QSGS are $c_d=0.01$ and $D_{1-4} : D_{5-8}=4:1$. The numerical results agree with the experimental data pretty well.

[Insert Figure 3 here]

The unsaturated porous media are then studied which involve three phases in one system. Customarily, the porosity, ε , is defined as the total volume fraction of the fluids. The degree of saturation, S , is defined as the liquid volume fraction within the fluids. Therefore the solid phase, the liquid phase and the gas phase have the volume fractions of $(1-\varepsilon)$, εS and $\varepsilon(1-S)$ respectively. Fig. 4 shows the predicted effective thermal conductivities versus the degree of saturation S for moist porous brick sands in both frozen and unfrozen states. The numerical results are compared again with the experimental data [52,53]. The QSGS parameters are $c_d=0.01$, $D_{1-4}:D_{5-8}=4:1$, $\varepsilon=0.52$ and $I_i^{3,2}=I_i^{3,3}$ for each i direction. The thermal conductivities used in the simulations are, $k_s=2.85$ W/m·K, $k_w=0.5924$ W/m·K, $k_g=0.0249$ W/m·K, and $k_{ice}=2.38$ W/m·K [53,54]. A 200×200 grid is used in the simulations, yielding the random fluctuation within 3%. Once again, good agreements are obtained with the experimental data for both frozen and unfrozen cases.

[Insert Figure 4 here]

4. Results and discussion

This section will focus on the phase distribution effects on the effective thermal conductivity of micro granular porous media by changing parameter values for the microstructure. Recently the three dimensional effects have been analyzed on the ETC of granular porous media and it was found that most experimental data measured by the hot probe and the hot agreed with the two dimensional predictions [22]. Since the hot probe and the hot wire are still most popular measurement methods for the ETC of granular porous media, our simulations in the present work focus on two-dimensional cases.

4.1 Pore/particle size effects

Several researchers have reported that the effective thermal conductivities of porous media may differ for different average pore/particle sizes by their experiments even though the components and the porosities of the media are same [55-58]. For the solid-air porous system, a finer solid particles medium

often led to a higher effective thermal conductivity at a same porosity [57,58]. This phenomenon can hardly be explained by the existing theoretical model for ETC, and few analyses have been found to focus on the mechanism so far.

Here we control the average pore/particle size by changing the values of c_d . A greater value of c_d leads to a smaller average size of pores/particles for a certain porosity ε . Fig. 5 demonstrates two generated structures at $\varepsilon=0.5$ where (a) has a ten times higher c_d than (b) does. The structure for a higher c_d looks more uniform and has a higher surface-to-volume ratio. The noisy surfaces of the generated structure could be regarded as a typical feature of natural granular porous media. The therefore complexities of structure may increase greatly computational costs of any classical PDE solvers, however, do not affect the computational efficiency of the LBM calculations much.

[Insert Figure 5 here]

After the porous structures are generated for different values of c_d , the particle size effect on ETC of porous media is then investigated. Fig. 6 shows the predicted ETC versus solid volume fraction ($1-\varepsilon$) for two different values of c_d . The thermal conductivities of the components are $k_s=3.0$ W/m·K and $k_g=0.025$ W/m·K. The theoretical solutions for Parallel mode and Series mode are also compared in the same figure. The results show that the ETC's of random porous media are between the values of Parallel mode and Series mode, and a larger average particle size leads to a lower ETC of porous media for all range of porosity except 0 and 1. The largest difference between ETCs for different values of c_d occurs when the solid volume fraction is within 0.5~0.8. Thus we keep the solid volume fraction at 0.5 and change the value of c_d . The predicted ETCs for different values of c_d are then shown in Fig. 7, which indicates the ETC value increases with the core distribution possibility. Since the particle average volume is inversely proportional to the value of c_d , the result means the ETC of porous media decreases monotonically with the particle average size.

[Insert Figure 6 here]

[Insert Figure 7 here]

To discuss the mechanism why a smaller average particle size leads to a higher ETC of porous media, we give the temperature fields for different structures in Fig. 8. The top and bottom boundaries are isothermal so that the temperature contours should be a series of uniform parallel lines for a homogeneous material. The temperature contours in the porous materials have been disturbed by the heterogeneous phase distributions, as shown in Fig. 8. However we still find that a larger value of c_d results in smoother temperature contours which are closer to those for homogeneous materials. Based on the uniformity principle of temperature gradient [59], the porous structure generated by a larger value of c_d deserves a higher ETC.

[Insert Figure 8 here]

4.2 Anisotropy effects

Most previous work has focused on the isotropic porous media. A few researchers generated anisotropic porous material by ellipse groups with different axis length or orientation angles [13]. Here we can achieve anisotropic phase distributions easily based on the QSGS process by varying values of the directional growth probability, D_i . No additional efforts are needed to deal with the inter-particle connections. Fig. 9 shows the generated structures for different ratio values of $D_x : D_y$, where D_x is the horizontal main directions (directions 1 and 3 in Fig. 1) and D_y is the vertical main directions (directions 2 and 4 in Fig. 1). The growth probabilities in the four diagonal directions are always set as a quarter of minimum of those in the main directions. The other parameters are $c_d=0.01$, $\varepsilon=0.5$ and the grid used is 200×200 . The generated microstructures show quite different characteristics for different values of directional growth probabilities. The anisotropy increases with the $D_x : D_y$ ratio. The directional growth probability corresponds to the macro structure statistical information, and can thus be determined by the measurement data from real porous structures.

[Insert Figure 9 here]

After the anisotropic microstructures are generated, we change the $D_x : D_y$ ratio from 0.01 to 100 and predict the effective thermal conductivity along the y direction. Fig. 10 shows the numerical results where $\varepsilon=0.5$, $c_d=0.01 \varepsilon$, $k_s=3.0$ W/m·K and $k_g=0.025$ W/m·K. The results indicate that the effective thermal conductivities along the y direction decrease monotonically with the $D_x : D_y$ ratio. For a given porosity, the effective thermal conductivity is enhanced along the direction with higher growth probability and meanwhile weakened along the direction with lower growth probability.

[Insert Figure 10 here]

4.3 Phase interaction effects

When a porous medium contains more than two phases, usually the multiphase interaction effects on the material properties have to be considered. For a three-phase porous system involving gas, liquid and solid, the simplest case is to generate the liquid phase with a uniform phase interaction growth probability, i.e. $I_i^{l,l} : I_i^{l,s} = 1$ with l representing the liquid phase and s the solid phase. This hypothesis is based on a strong wetting effect caused by a strong liquid-solid attractive potential, and will result in a uniform liquid film attached on the solid grains as shown in Fig. 11-a. The smaller is the $I_i^{l,l} : I_i^{l,s}$ ratio, the more uniform is the liquid film (see Fig. 11-b). Such structures can be found in some multi-components composite materials [17]. However for the unsaturated sandstones or glass assemblies, the wetting characteristic of water may be different. Both the lowest interface energy law [20] and the measured images [60] have shown that the water in sandstones or glass assemblies tends to be in conglomeration rather than in films on the solid surfaces due to the weak wetting properties. Here we reproduce the water distributions similar to those in sandstones or glass assemblies by changing the values of $I_i^{l,l} : I_i^{l,s}$ ratio, as shown in Fig. 11-c and d. Now Fig. 11 compares the water distributions in the porous media for different phase interaction growth probabilities. The solid phase distributions are isotropic with the

volume fraction $\varepsilon=0.5$ and the core distribution probability $c_d=0.01\varepsilon$. The water volume fraction is 0.25 and the $I_i^{l,l}:I_i^{l,s}$ ratio changes from 10:1 to 1:100. A greater value of the $I_i^{l,l}:I_i^{l,s}$ ratio means a weaker liquid-solid interphase attractive potential and a weaker wetting interface, i.e., the liquid will be more aggregative as a result.

[Insert Figure 11 here]

The phase interaction growth probability effects on the ETC of multiphase porous media are thus studied. Assuming an unsaturated sandstone case where the solid particle volume fraction is $\varepsilon=0.5$ with $c_d=0.01\varepsilon$, the water volume fraction is $P_l=0.3$, and the component thermal conductivities are $k_s=3.0$ W/m K, $k_l=0.1$ W/m K, and $k_g=0.025$ W/m K respectively. Fig. 12 shows the predicted ETC for different liquid-solid phase interaction growth probabilities. The results indicate that the ETC of multiphase porous media increases with the degree of liquid phase conglomeration. The calculated ETC changes little when the $I_i^{l,l}:I_i^{l,s}$ ratio is less than 1, and increases remarkably when the $I_i^{l,l}:I_i^{l,s}$ ratio is greater than 10.

[Insert Figure 12 here]

5. Conclusions

To model and analyze the phase distribution effects on the effective thermal conductivity of multiphase porous media, we have developed the Quartet Structure Generation Set (QSGS) for generating different kinds of multiphase granular porous structures and the lattice Boltzmann method (LBM) for solving the energy transport equations efficiently with multiphase conjugate effects considered. The numerical algorithms have been validated by a series of comparisons with existing theoretical solutions and experimental data.

The phase distribution characteristics were controlled by the parameters of QSGS and the effective thermal conductivities for various distributed porous media were then calculated by the LBM. The results showed that a smaller average particle size could lead to a better uniformity of phase distribution and a

larger surface-to-volume ratio, both of which would result in a more uniform temperature gradient field for same temperature differences. Therefore the smaller is the average particle size, the larger is the effective thermal conductivity for a certain porosity, which agrees with the existing experimental phenomena. The anisotropy of porous media is controlled by the directional growth probability. If the larger directional growth probability is along the direction of temperature gradient, the ETC in this direction will be enhanced. As a result, the ETC in the vertical direction will be weakened. For three or more phase porous media, the degree of phase conglomeration is determined by the phase interactions, such as wetting properties. A larger liquid-liquid interaction leads to a higher degree of liquid phase conglomeration. The numerical results showed that the ETC of multiphase porous media increases with the degree of liquid phase conglomeration.

Acknowledgements

The present work is supported by a grant from the NTC-M04-CD01 and NSF-061308 of USA and the NSF (59995550-2) of China.

References

- [1] R.W. Zimmerman. Thermal Conductivity of Fluid-Saturated Rocks. *J. Petroleum Sci. Engin.* **3**: 219-227, 1989
- [2] R.W. Zimmerman. *Compressibility of Sandstones*. Elsevier Science Pub. Co. New York, 1991
- [3] M. Quintard and M. Todorović. *Heat and mass transfer in porous media*. Elsevier Science Pub. Co. New York, 1992
- [4] A. Verruijt. *Computational geomechanics*. Kluwer Academic, Boston, 1995
- [5] D.B. Ingham, A. Bejan, E. Mamut, and I. Pop. *Emerging Technologies and Techniques in Porous Media*. Kluwer Academic Publishers. London, 2003
- [6] G.Q. Lu and X.S. Zhao. *Nanoporous Materials-Science and Engineering, Chemical Engineering Series*, Imperial College Press, London, 2004
- [7] D.B. Ingham, and I. Pop. *Transport Phenomena in Porous media III*, Elsevier Science Pub. Co., Oxford, UK, 2005
- [8] A. Sayari and M. Jaroniec. *Nanoporous Materials IV*. Elsevier Science Pub. Co., New York, 2005
- [9] A. Bouguera Prediction of effective thermal conductivity of moist wood concrete. *J. Phys. D: Appl. Phys.* **32**: 1407-1414, 1999
- [10] X.G. Liang, and W. Qu. Effective thermal conductivity of gas-solid composite materials and the temperature difference effect at high temperature. *Int. J. Heat Mass Transfer.* **42** (10): 1885-1893, 1999
- [11] J.E.J. Staggs. Estimating the thermal conductivity of chars and porous residues using thermal resistor networks. *Fire Safety Journal.* **37** (1): 107-119, 2002
- [12] J.F. Wang, J.K. Carson, M.F. North, and D.J. Cleland. A new approach to modeling the effective thermal conductivity of heterogeneous materials. *Int. J. Heat Mass Transfer.* **49**: 3075-3083, 2006
- [13] L. Tacher, P. Perrochet, and A. Parriaux. Generation of granular media. *Transport in Porous Media.* **26** (1): 99-107, 1997
- [14] M. Pilotti. Generation of realistic porous media by grains sedimentation. *Transport in Porous Media.* **33** (3): 257-278, 1998
- [15] K. Makrodimitris, G.K. Papadopoulos, C. Philippopoulos, and D.N. Theodorou. Parallel tempering method for reconstructing isotropic and anisotropic porous media. *J. Chem. Phys.* **117**: 5876-5884, 2002
- [16] D.S. Li, G. Saheli, M. Khaleel, and H. Garmestani. Quantitative prediction of effective conductivity in anisotropic heterogeneous media using two-point correlation functions. *Comput. Mat. Sci.* **38** (1): 45-50, 2006
- [17] N. Losic, J.F. Thovert, and P.M. Adler. Reconstruction of Porous Media with Multiple Solid Phases. *J. Colloid Interface Sci.* **186**: 420-433, 1997
- [18] S. Torquato. *Random heterogeneous materials: microstructure and macroscopic properties*. New York : Springer, 2002

- [19] S. Torquato. Modeling of physical properties of composite materials. *Int. J. Solids Structures*. **37**: 411-422, 2000
- [20] S. Mohanty. Effect of multiphase fluid saturation on the thermal conductivity of geologic media. *J. Phys. D: Appl. Phys.* **30**: L80-L84, 1997
- [21] M. Wang, J.K. Wang, N. Pan, and S.Y. Chen. Mesoscopic Predictions of the Effective Thermal Conductivity of Microscale Random Porous Media. *Phys. Rev. E.*, **75**: 036702, 2007
- [22] M. Wang, J.K. Wang, N. Pan, S.Y. Chen, and J.H. He. Three dimensional effect on the effective thermal conductivity of porous media. *J. Phys. D: Appl. Phys.* **40**: 260-265, 2007
- [23] P. Meakin. *Fractals, scaling and growth far from equilibrium*. Cambridge University Press, 1998
- [24] J.F. Thovert, F. Wary and P.M. Adler. Thermal Conductivity of Random Media and Regular Fractals. *J. Appl. Phys.* **68**: 3872-3883, 1990
- [25] D. Coelho, J.F. Thovert and P.M. Adler. Geometrical and transport properties of random packings of spheres and aspherical particles. *Phys. Rev. E* **55** (2): 1959-1978, 1997
- [26] K. Bakker. Using the finite element method to compute the influence of complex porosity and inclusion structures on the thermal and electrical conductivity *Int. J. Heat Mass Transfer* **40** (15): 3503-3511, 1997
- [27] A.G. Fedorov and R.Viskanta. Three-dimensional conjugate heat transfer in the microchannel heat sink for electronic packaging, *Int. J. Heat Mass Transfer*. **43**: 399-415, 2000
- [28] A. Horvat and I. Catton. Numerical technique for modeling conjugate heat transfer in an electronic device heat sink. *Int. J. Heat Mass Transfer*. **46**: 2155-2168, 2003
- [29] D.X. Zhang. *Stochastic Method for Flow in Porous Media*. Academic Press. London. 2002
- [30] D. Kulasiri and W. Verwoerd. *Stochastic Dynamics Modeling Solute Transport in Porous Media*. Elsevier. New York. 2002
- [31] Y. Shoshany, D. Prialnik, M. Podolak. Monte Carlo Modeling of the thermal conductivity of porous cometary ice. *Icarus* **157** (1): 219-227, 2002
- [32] S. Barta and P. Dieska. Effective thermal conductivity of particulate composite materials *Kovove Materialy-Metallic Materials* **40** (2): 99-112, 2002
- [33] H.F. Zhang, X.S. Ge and H. Ye. Effectiveness of the heat conduction reinforcement of particle filled composites *Modelling and Simulation in Materials Science and Engineering*. **13** (3): 401-412, 2005
- [34] H.F. Zhang, X.S. Ge and H. Ye. Randomly mixed model for predicting the effective thermal conductivity of moist porous media. *J. Phys. D: Appl. Phys.* **39** (1): 220-226, 2006
- [35] J.Y. Qian, Q. Li, K. Yu and Y.M. Xuan. A novel method to determine the effective thermal conductivity of porous materials. *Sci in China Ser. E.*, **47**: 716-724, 2004
- [36] X. Chen and P. Han. A note on the solution of conjugate heat transfer problems using SIMPLE-like algorithms. *Int. J. Heat Fluid Flow*. **21**: 463-467, 2000
- [37] J.K. Wang, M. Wang, and Z.X. Li. A Lattice Boltzmann Algorithm for Fluid-Solid Conjugate Heat Transfer. *Int. J. Thermal Sci.* **46**(3) 228-234, 2007

- [38] X. He and L.S. Luo. A priori derivation of the lattice Boltzmann equation. *Phys. Rev. E*. **55**: 6333-6336, 1997
- [39] T. Abe. Derivation of the lattice Boltzmann method by means of the discrete ordinate method for the Boltzmann equation. *J. Comp. Phys.* **131**: 241-246, 1997
- [40] S.Y. Chen, G.D. Doolen. Lattice Boltzmann method for fluid flows, *Annu. Rev. Fluid Mech.* **30**: 329-364, 1998
- [41] D. Raabe. Overview of the lattice Boltzmann method for nano- and micorscale flow dynamics in materials science and engineering. *Modelling Simul. Mater. Sci. Eng.* **12**: R13-R46, 2004
- [42] J.K. Wang, M. Wang, Z.X. Li. Lattice Poisson-Boltzmann Simulations of Electro-osmotic Flows in Microchannels, *J. Colloid Interface Sci.* **296**: 729-736, 2006
- [43] M. Wang, J.K. Wang, Z.X. Li. Lattice Poisson-Boltzmann simulations of electro-osmotic flows in microchannels (vol 296, pg 729, 2006). *J. Colloid Interface Sci.* **300** (1): 446-446, 2006
- [44] Q.J. Kang, D.X. Zhang, S.Y. Chen. Simulation of dissolution and precipitation in porous media, *J. Geophys. Res.* **108**: 2505, 2003
- [45] Q.J. Kang, D.X. Zhang, P.C. Lichtner. Tsimpanogiannis I.N., Lattice Boltzmann model for crystal growth from supersaturated solution, *Geophys. Res. Lett.* **31**: L21604, 2004
- [46] M. Wang, J.K. Wang, S.Y. Chen, and N. Pan. Electrokinetic Pumping Effects of Charged Porous Media in Microchannels using the Lattice Poisson-Boltzmann Method. *J. Colloid Interface Sci.* **304**(1): 246-253, 2006
- [47] S. Succi. *The Lattice Boltzmann Equation for Fluid Dynamics and Beyond*, Oxford Science Press, London, 2001
- [48] X.Y. He, S.Y. Chen, G.D. Doolen. A novel thermal model for the lattice Boltzmann method in incompressible limit, *J. Comput. Phys.* **146**: 282-300, 1998
- [49] Y. Peng, C. Shu, Y. T. Chew, Simplified thermal lattice Boltzmann model for incompressible thermal flows, *Phys. Rev. E*. **68**: 026701, 2003
- [50] Q.S. Zou, X.Y. He. On pressure and velocity boundary conditions for the lattice Boltzmann BGK model. *Phys. Fluids* **9** (6): 1591-1598, 1997
- [51] H.J. Lee and R.E. Taylor. Thermal diffusivity of dispersed composites. *J. Appl. Phys.* **47**(1): 148-151, 1976
- [52] A.R. Sepaskhah and L. Boersma. Thermal-conductivity of soils as a function of temperature and water-content. *Soil Sci. Soc. Am. J.*, **43** (3): 439-444, 1979
- [53] A.K. Singh, R. Singh and D.R. Chaudhary Prediction of effective thermal conductivity of moist porous materials. *J. Phys. D: Appl. Phys.*, **23**(6): 698-702, 1990
- [54] S. Fukusako Thermophysical properties of ice, snow and sea ice. *Int. J. Thermophys.* **11**(2): 353-372, 1990
- [55] G. N. Dulnev, D. P. Volkov and A. B. Utkin. Effective thermal conductivity of moistened porous bodies. *Journal of Engineering Physics and Thermophysics*, **52**(2): 213-217, 1987
- [56] V.V. Polyakov, M.A. Utemesov and A.V. Egorov. Influence of Structure on the Thermophysical Characteristics of Porous Metals. *Journal of Engineering Physics and Thermophysics*, **68**(5): 580-583, 1995

- [57] K. Midttomme, E. Roaldset. The effect of grain size on thermal conductivity of quartz sands and silts. *Petroleum Geoscience* **4** (2): 165-172, 1998
- [58] J.Z. Liang, F.H. Li. Measurement of thermal conductivity of hollow glass-bead-filled polypropylene composites. *Polymer Testing*. **25** (4): 527-531, 2006
- [59] X.G. Cheng, Z.X. Li, Z.Y. Guo. Constructs of highly effective heat transport paths by bionic optimization. *Sci. China. Ser. E* **46** (3): 296-302, 2003
- [60] S. Torquato. Statistical descriptions of microstructures. *Annu. Rev. Mater. Res.* **32**:77–111, 2002

Tables

$k_1 : k_2$	Mode	Theoretical value (W/m K)	Numerical value (W/m K)	Deviation (%)
1:2	Parallel	1.500	1.500	0.000
	Series	1.333	1.332	0.075
1:10	Parallel	5.500	5.500	0.000
	Series	1.818	1.814	0.220
1:100	Parallel	50.50	50.50	0.000
	Series	1.980	1.975	0.250
1:500	Parallel	250.5	250.5	0.000
	Series	1.996	1.991	0.250
1:1000	Parallel	500.5	500.4	0.020
	Series	1.998	1.993	0.250

Figure Captions

Fig. 1 Eight growth directions of each point for 2D systems

Fig. 2 Two basic structures for validation

Fig. 3 Comparisons between predictions and experimental data for Cu/solder material. The experimental data is from Ref. [51]. The parameters are $k_{Cu}=398.0$ W/m K and $k_{solder}=78.1$ W/m K.

Fig. 4 Comparisons between predicted and experimental effective thermal conductivities of unsaturated porous sands in frozen and unfrozen states. The experimental data is from Ref. [52,53]. The parameters are $\varepsilon=0.52$, $k_s=2.85$ W/m·K, $k_w=0.5924$ W/m·K, $k_g=0.0249$ W/m·K, and $k_{ice}=2.38$ W/m·K

Fig. 5 Structures for different values of c_d at a same porosity $\varepsilon=0.5$. The directional parameters are set as: $D_{1-4} : D_{5-8}=4:1$. The dark is gas and the white is solid.

Fig. 6 ETC versus solid volume fraction for different values of c_d .

Fig. 7 ETC versus value of c_d at $\varepsilon=0.5$

Fig. 8 Temperature contours for different values of c_d

Fig. 9 Microstructures of anisotropic porous media with different directional growth probabilities with $c_d=0.01$, $\varepsilon=0.5$. The dark is gas and the white is solid.

Fig. 10 ETC of anisotropic porous media for different directional growth probabilities

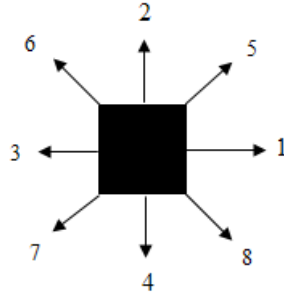


Fig. 1 Eight growth directions of each point for 2D systems

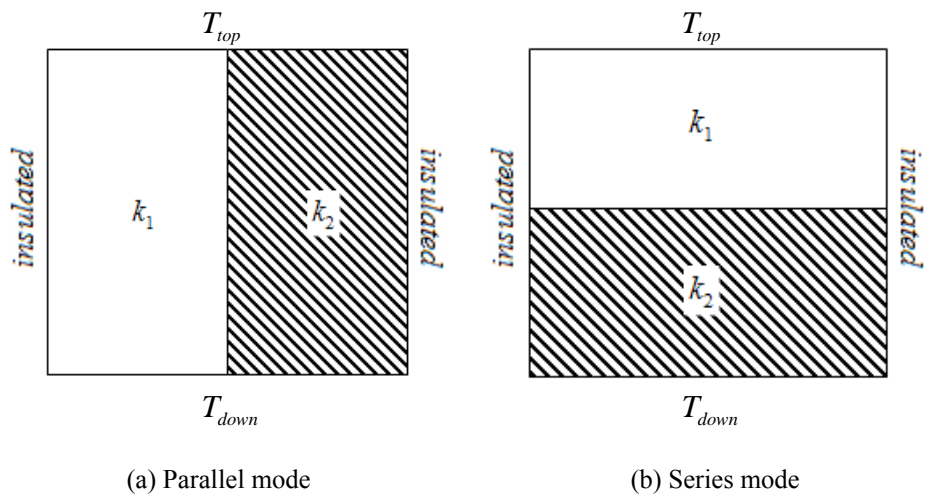


Fig. 2 Two basic structures for validation

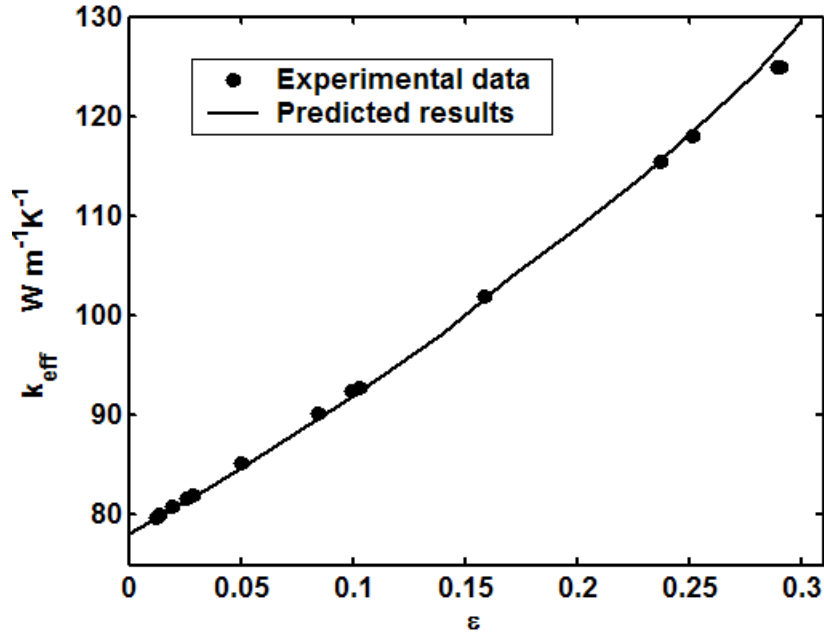


Fig. 3 Comparisons between predictions and experimental data for Cu/solder material. The experimental data is from Ref. [51]. The parameters are $k_{Cu}=398.0$ W/m K and $k_{solder}=78.1$ W/m K.

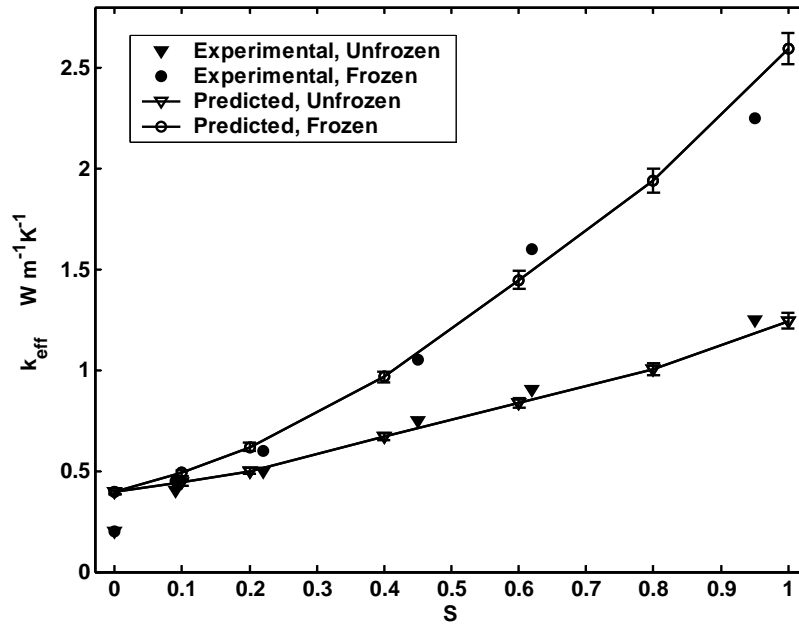
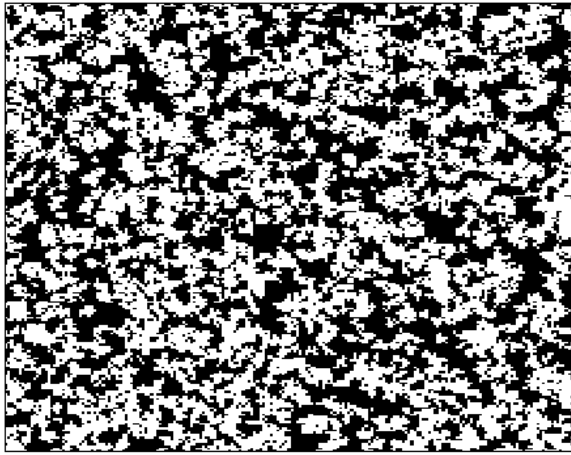
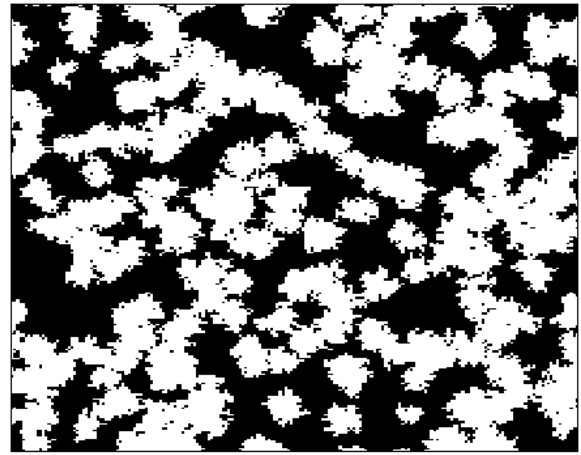


Fig. 4 Comparisons between predicted and experimental effective thermal conductivities of unsaturated porous sands in frozen and unfrozen states. The experimental data is from Ref. [52,53]. The parameters are $\epsilon=0.52$, $k_s=2.85$ W/m·K, $k_w=0.5924$ W/m·K, $k_g=0.0249$ W/m·K, and $k_{ice}=2.38$ W/m·K



(a) $c_d = 0.1 \varepsilon$



(b) $c_d = 0.01 \varepsilon$

Fig. 5 Structures for different values of c_d at a same porosity $\varepsilon = 0.5$. The directional parameters are set as: $D_{1-4} : D_{5-8} = 4:1$. The dark is gas and the white is solid.

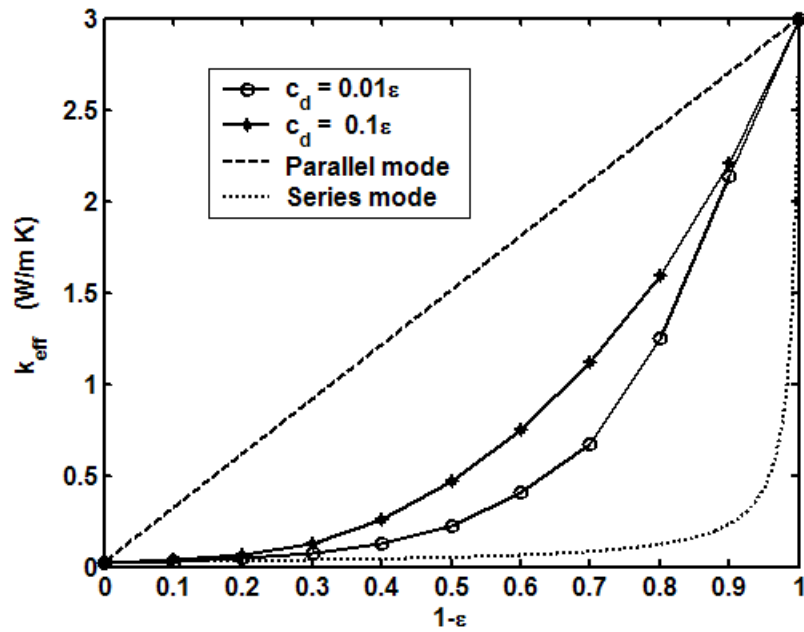


Fig. 6 ETC versus solid volume fraction for different values of c_d .

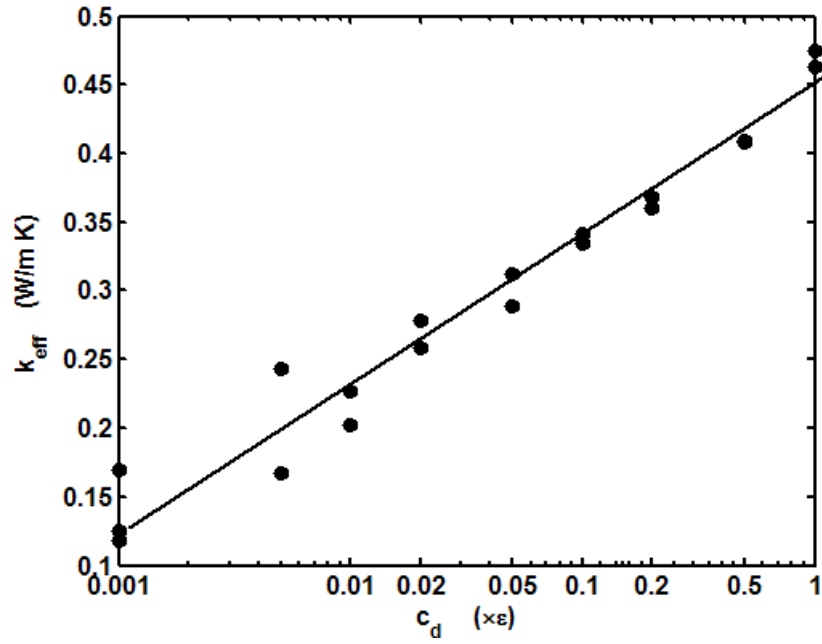
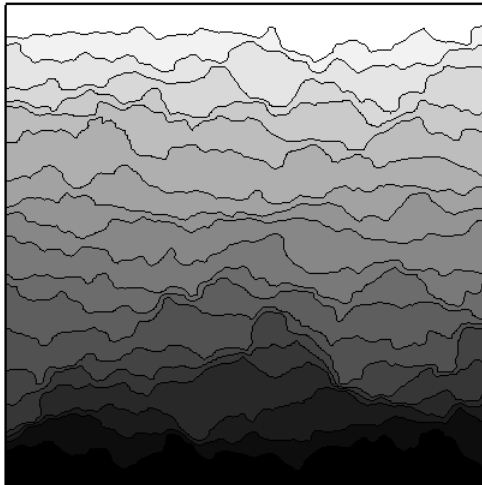
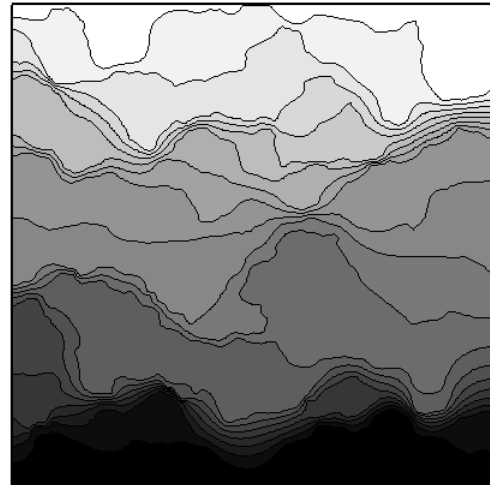


Fig. 7 ETC versus value of c_d at $\epsilon=0.5$

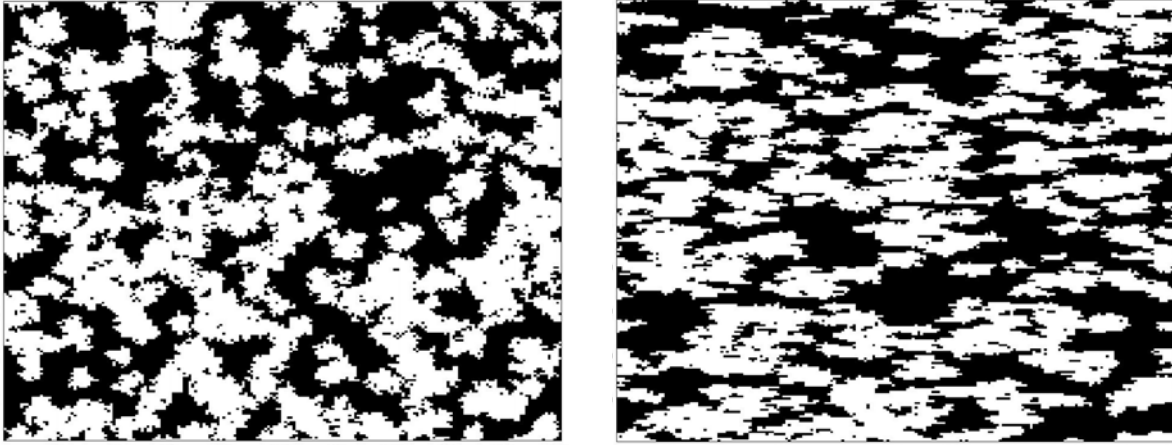


(a) $c_d = 0.1 \epsilon$



(b) $c_d = 0.01 \epsilon$

Fig. 8 Temperature contours for different values of c_d



(a) $D_x : D_y = 1:1$

(b) $D_x : D_y = 10:1$

Fig. 9 Microstructures of anisotropic porous media with different directional growth probabilities with $c_d=0.01$, $\varepsilon=0.5$. The dark is gas and the white is solid.

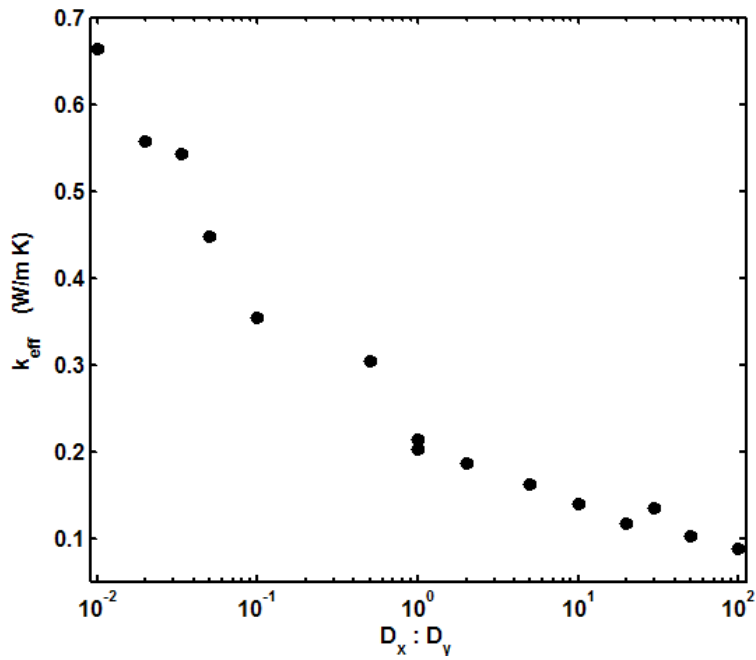
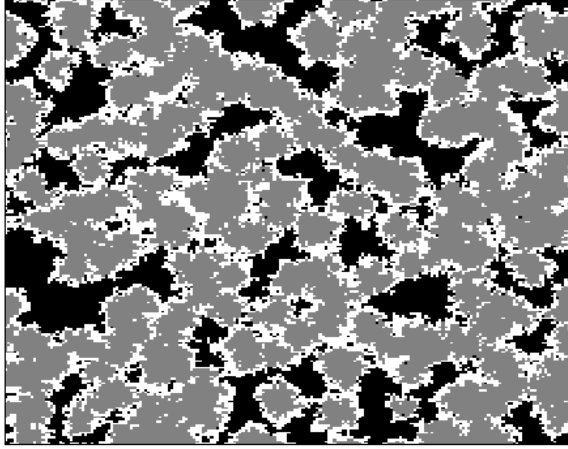
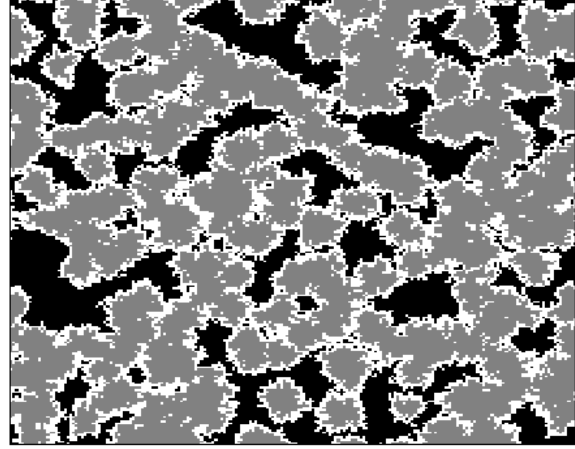


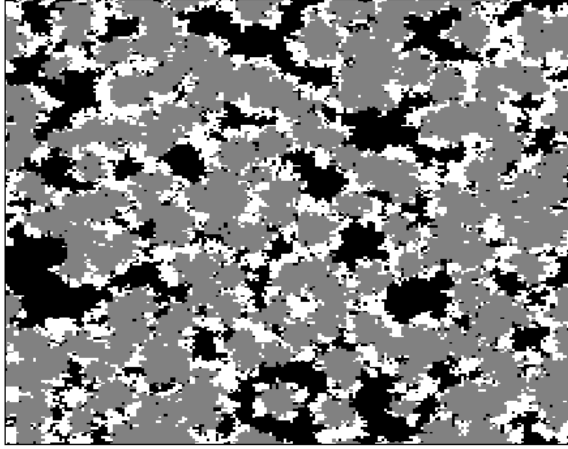
Fig. 10 ETC of anisotropic porous media for different directional growth probabilities



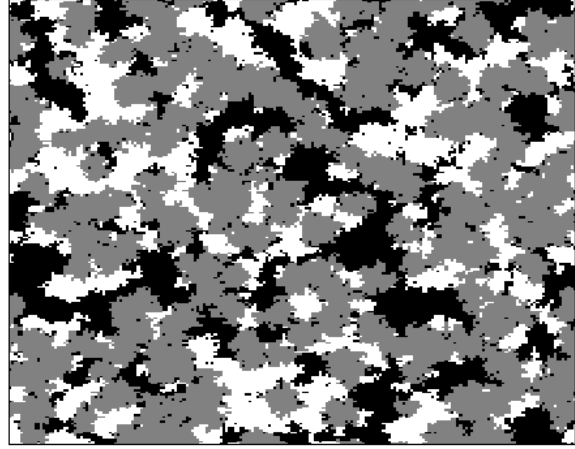
(a) $I_i^{l,l} : I_i^{l,s} = 1:1$



(b) $I_i^{l,l} : I_i^{l,s} = 1: 10$



(c) $I_i^{l,l} : I_i^{l,s} = 10:1$



(d) $I_i^{l,l} : I_i^{l,s} = 100: 1$

Fig. 11 Microstructures of 3-phase porous media with different phase interaction growth probabilities. The gray is solid particles, the white is liquid, and the dark is gas. The solid is isotropic with $c_d = 0.01 \varepsilon$. The porosity $\varepsilon (P_2) = 0.5$, and the liquid volume fraction $P_l = 0.25$.

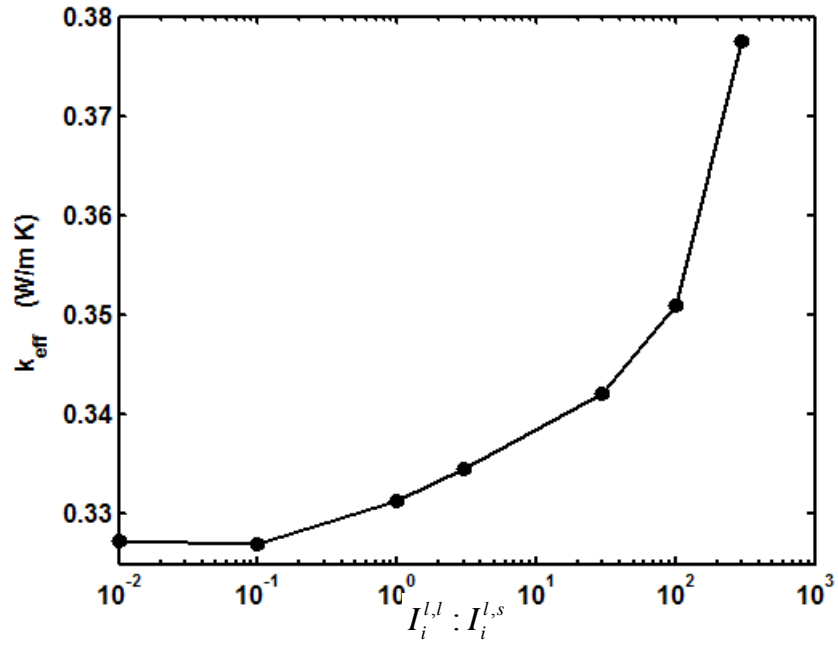


Fig. 12 ETC of three-phase porous media for different liquid-solid phase interaction growth probabilities. The parameters are: $\varepsilon=0.5$, $c_d=0.01 \varepsilon$, $P_l=0.3$, $k_s=3.0$ W/m K, $k_l=0.1$ W/m K, and $k_g=0.025$ W/m K.